Threshold Voltage and Space Charge in Organic Transistors

I. Gutiérrez Lezama and A. F. Morpurgo
DPMC and GAP, Université de Genéve, 24 quai Ernest Ansermet, CH1211 Geneva, Switzerland

(Received 28 April 2009; published 6 August 2009)

We investigate rubrene single-crystal field-effect transistors, whose stability and reproducibility are sufficient to measure systematically the shift in threshold voltage as a function of channel length and source-drain voltage. The shift is due to space charge transferred from the contacts and can be modeled quantitatively without free fitting parameters, using Poisson's equation, and by assuming that the density of states in rubrene is that of a conventional inorganic semiconductor. Our results demonstrate the consistency, at the quantitative level, of a variety of recent experiments on rubrene crystals and show how the use of field-effect transistor measurements can enable the determination of microscopic parameters (e.g., the effective mass of charge carriers).

DOI: 10.1103/PhysRevLett.103.066803 PACS numbers: 73.40.−c, 73.61.Ph

Organic single-crystal field-effect transistors (FETs) are opening new possibilities for the detailed investigation of the intrinsic electronic properties of organic semiconductors and of their interfaces [1,2]. Transistors where a single crystal was suspended on top of a gate electrode have led to the observation of intrinsic transport properties, such as mobility anisotropy [3] and metalliclike temperature dependence [4]. Current work is aimed at the systematic study of microscopic electronic processes in these systems. Examples are the study of polaronic effects at the interface between organic crystals and highly polarizable dielectrics [5–7], the analysis of bandlike transport at interfaces with low-ϵ materials [8,9], and the detailed investigation of electronic transport at metal-organic interfaces [10]. In most cases, a quantitative analysis of the data in terms of well-defined microscopic models has been possible, but the consistency of results obtained in different experiments remains to be verified.

Virtually all experiments on single-crystal FETs have focused on transport through a well-formed conducting channel, i.e., in the regime when the gate voltage is biased well above the threshold voltage V_T. Here we use rubrene single-crystal FETs for a systematic experimental investigation of the behavior of the threshold voltage itself. Specifically, we have measured the electrical characteristics of short-channel transistors as a function of channel length L and extracted the dependence of V_T on L and on source-drain bias V_{DS}. We find that V_T systematically shifts to more positive values when L is decreased or V_{DS} is increased, a behavior originating from changes in the space charge transferred from the contacts into the semiconductor. We model the system using Poisson's equation, under the assumption that the density of states in the molecular crystals has the same functional dependence as in inorganic semiconductors, and find excellent quantitative agreement between experimental data and calculations, without introducing any adjustable parameter. Our results indicate that the effective mass of carriers in the rubrene valence band is close to the free electron mass, provide information about the low-energy density of states, and show that the physical picture used to interpret a variety of recent experiments [10,11] is internally consistent at a quantitative level.

Not much is currently known about the microscopic processes determining the behavior of the threshold voltage in organic transistors. Work done on thin-film devices has established that this behavior can be complex, exhibiting large sample-to-sample fluctuations and instabilities [12]. These phenomena have so far prevented systematic experiments and are posing severe technological problems. The situation appears to be different in single-crystal devices, with recent work showing considerably better reproducibility [13].

The fabrication of the rubrene FETs relies on the lamination of thin (≤ 1 μm-thick) single crystals on top of a highly doped silicon substrate (acting as a gate) covered with 500 nm SiO_2, with predefined oxidized copper electrodes [14]. The devices are identical to those that we used previously for the investigation of the contact resistance and are therefore very well characterized [10,15]. In that work we focused on the high-gate voltage regime with a fully formed channel; here we analyze the behavior of the threshold voltage V_T.

Transport measurements were performed at room temperature, in the dark, and in vacuum ($2–7 \times 10^{-7}$ mbar), using a HP4156A parameter analyzer. Owing to the short-channel length, the resistance of the devices is dominated by the contacts, resulting in the characteristic (sublinear) shape [10] of the transfer curves seen in Figs. 1(c) and 2. Special care was taken in restricting the applied gate voltage V_G to the narrowest possible range around V_T, to suppress possible effects of bias stress. Accordingly, the output characteristics of our devices are hysteresis-free, with stable and reproducible V_T values. To extract these values, we have used the linear extrapolation method and fitted the linear regime of the transfer curve that follows the

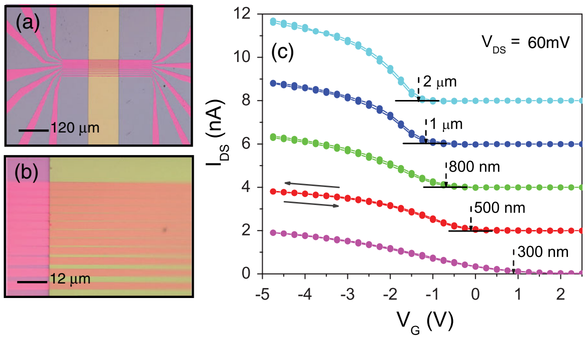

FIG. 1 (color online). Panels (a) and (b) show optical microscope images of devices used in this work. Panel (c) shows the transfer characteristics of FETs with different channel lengths, measured at $V_{DS} = 60$ mV (the curves are offset vertically for clarity). The sublinear V_G dependence is characteristic of contact dominated devices [10]. The vertical arrows point to the position of the threshold voltage in different devices. The two arrows with a continuous line indicate that for each data set the gate voltage is swept up and down.

onset of conduction (as illustrated in the inset of Fig. 2). The uncertainty on the V_T values extracted using this method is at most ±0.1 V (for the shortest devices) and usually better.

The behavior of the threshold voltage as a function of channel length L and bias V_{DS} is apparent from Figs. 1(c) and 2. Figure 1(c) shows the transfer characteristics of transistors with different channel lengths, measured at the same value of V_{DS}. It is apparent that V_T systematically shifts to more positive values in devices with a shorter channel. Figure 2 shows measurements done on an individual transistor for increasing values of V_{DS}. A shift of V_T to positive values (see Fig. 3) is clearly present, which is found to be larger for shorter devices. These trends resemble those recently reported in Ref. [13]. Figure 3 provides a complete overview of the behavior of V_T in our experiments. The different devices (i.e., sets of FETs with different channel length fabricated on the same crystal) investigated exhibited identical trends and similar magnitude of the observed effects.

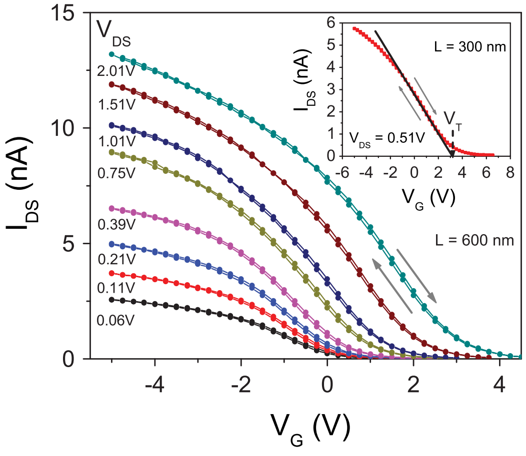

FIG. 2 (color online). Transfer characteristics of a rubrene single-crystal FET with channel length $L = 600$ nm, measured for different values of the source-drain voltage V_{DS}. The arrows indicate that in all measurements the gate voltage has been swept up and down. The inset illustrates how the threshold voltage is extracted from the data.

The shift of V_T as a function of L and V_{DS} originates from the transfer of charge from the source and drain contacts into the semiconductor. At low V_{DS} (i.e., $V_{DS} \simeq kT/e$), charge transfer occurs to align the Fermi level in the metal and in the bulk of the semiconductor. As the contact separation is decreased, the corresponding charge density in the (bulk) region of the semiconductor between source and drain contact increases. At finite V_{DS}, additional charge is transferred from the contacts to the semiconductor due to capacitive coupling, similarly to what happens in space-charge limited current measurements [16]. As charge density and potential are linked by Poisson's equation, the transferred charge induces a shift in the electrostatic potential, which needs to be compensated by a shift in the threshold voltage to switch off conduction. In simpler terms, to switch off conduction, the space charge transferred from the electrodes into the bulk of the semiconductor needs to be compensated by an equal and opposite amount of charge accumulated in the channel (i.e., by a shift in V_T).

At a quantitative level, we consider the case of low-bias first, and we calculate the profile of charge density transferred from the electrodes into the bulk of the semiconductor [Fig. 4(a)] by solving the Poisson equation. To this end, we employ a one-dimensional (1D) model, to describe how electrostatic potential $\Phi_s(x)$ and charge density $\rho_s(x)$ vary in the bulk of the semiconductor, away from an interface with a metal contact [Fig. 4(b)]. We then have

$$\frac{d^2\Phi_s(x)}{dx^2} = \frac{q\rho_s(x)}{\epsilon_0\epsilon_C} = \frac{q}{\epsilon_0\epsilon_C} M_H e^{-q\Phi_s(x)/kT}. \qquad (1)$$

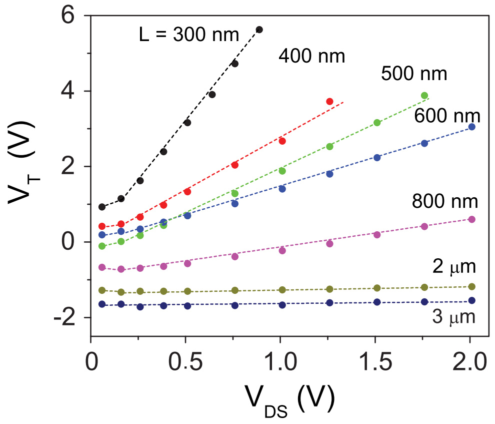

FIG. 3 (color online). The dots represent V_T values of short-channel single-crystal devices as a function of V_{DS} measured on devices with different channel length L (the dotted lines are guides for the eye).

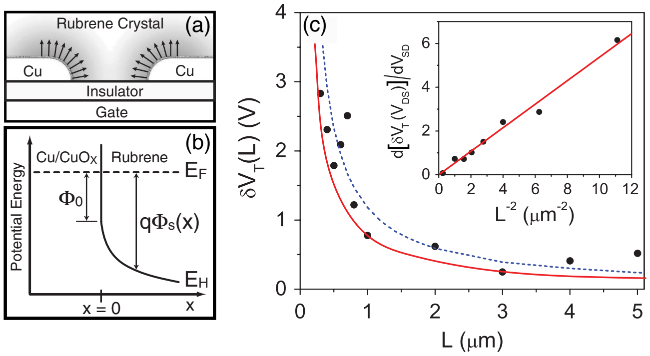

FIG. 4 (color online). Panel (a) shows schematics of the region between the source and drain contacts of a FET device. The arrows indicate charge transfer from the contacts into the semiconductor; the transferred charge is represented by the shaded region. Panel (b) shows the potential energy band diagram near one metal-rubrene interface. Panel (c) shows the comparison between the measured $\delta V_T(L)$ and the values calculated using Poisson's equation. The blue dotted line and the red line represent the values calculated with $\Phi_0 = 0.13$ and 0.15 eV, respectively (corresponding to the known range of measured values for the CuO_x/rubrene interface). The inset shows that $d[\delta V_T(V_{DS})]/dV_{DS}$ scales linearly with L^{-2}.

Here $M_H = 2(2\pi m_p kTh^{-2})^{3/2}$, with m_p the effective mass of holes in the "highest occupied molecular orbital" band of rubrene (i.e., the valence band of the organic semiconductor), ϵ_0 the vacuum permittivity, and ϵ_C the relative dielectric constant of rubrene. The last equality assumes that the density of states in rubrene has the same dependence as in a conventional one-band semiconductor, i.e., a parabolic dispersion relation with an effective mass m_p, which allows expression of the local density of charge carriers $\rho_s(x)$ as a function of the local potential $\Phi_s(x)$ [17]. Clearly, the validity of this hypothesis needs to be checked by comparing the results of the calculations to the experimental data.

There are two boundary conditions associated to Poisson's equation. The first, $\Phi_s(0) = \Phi_0/q$, fixes the constant in the potential so that $q\Phi_s(x)$ corresponds to the local distance between the Fermi level and the valence band edge in the semiconductor (Φ_0 is the energy difference between the metal Fermi level and the valence band edge; when a large gate voltage is applied, Φ_0 corresponds to the height of the Schottky barrier present at the metal-semiconductor interface). The second is $d\Phi_s/dx|_{x\to\infty} = 0$, which imposes that the electric field vanishes in the bulk of the semiconductor, far away from the interface with the metal. Under these conditions, the solution to Poisson's equation is

$$\Phi_s(x) = \frac{2kT}{q}\ln\left[e^{\Phi_0/2kT} + x\sqrt{\frac{q^2 M_H}{2kT\epsilon_0\epsilon_C}}\right], \qquad (2)$$

and the corresponding charge carrier density is given by

$$\rho_s(x) = qM_H\left[e^{\Phi_0/2kT} + x\sqrt{\frac{q^2 M_H}{2kT\epsilon_0\epsilon_C}}\right]^{-2}. \qquad (3)$$

Note that in Eq. (1) we have neglected "bulk" contributions to the charge density, e.g., due to (unintentionally present) dopants or thermally activated charge carriers. Accordingly, Eqs. (2) and (3) are valid inside the semiconductor, only at a small distance from the electrode surface, where the charge transferred from the contacts is larger than the one present due to dopants, which in high-purity crystals is $N_D \approx 2\times 10^{14}\ \mathrm{cm}^{-3}$ [18]. This value is much smaller than what is usually found in organic semiconductors, and hence in our devices the space charge penetrates deeper into the rubrene crystals. By using Eq. (3), with $\Phi_0 = 0.13$–0.15 eV [10] (see discussion below) and taking into account the overlapping of the space-charge regions coming from both contacts, it is easy to verify that the charge transferred from the contacts is larger than N_D even for devices with $L \simeq 1\ \mu\mathrm{m}$ (normally, due to the large doping in organic semiconductors, this length is only a few tenths of a nanometer [19]).

To link the calculated quantities to the data, we impose that the total amount of space charge transferred from the contacts into the bulk region of the semiconductor between source and drain contacts is compensated, at threshold, by an equal and opposite amount of charge accumulated in the channel [i.e., by a shift in threshold voltage $\delta V_T(L)$]. We then get

$$\begin{aligned}\delta V_T(L) &= \frac{qt_C\langle\rho_s(L)\rangle}{C_G}\\ &= \frac{2qt_C M_H}{C_G}\left[e^{\Phi_0/kT} + Le^{\Phi_0/2kT}\sqrt{\frac{q^2 M_H}{2kT\epsilon_0\epsilon_C}}\right]^{-1},\end{aligned} \qquad (4)$$

where $\langle\rho_s(L)\rangle$ is the spatial average of the carrier density present in the overlapping space-charge regions originating from the two contacts, C_G is the gate capacitance per unit area, and t_C is the thickness of the rubrene crystal (measured with a profilometer). This estimate of δV_T is approximate, in that our calculation does not take into account the precise geometry. For our devices, we estimate that the error is a geometrical factor of the order of unity (see the below discussion on the V_{DS} dependence of δV_T).

Figure 4(c) shows the comparison between the predictions of Eq. (4) and the measured values $\delta V_T(L) = V_T(L) - \langle V_T\rangle$ (where $\langle V_T\rangle = -1.9$ V is the average threshold voltage obtained from devices with $10\ \mu\mathrm{m} \le L \le 50\ \mu\mathrm{m}$; all measurements were performed at $V_{DS} = 60$ mV). The lines represent the results of the calculations using the values of Φ_0 for a CuO_x/rubrene interface, known from our study of the contact resistance: Φ_0 typically varies between 0.13 and 0.15 eV in different devices [20]. For the hole effective mass m_p, we take the value extracted from recent optical spectroscopy experiments, which is close to the free electron mass [11]. All other quantities in the theoretical expression are known, and there are no free adjustable parameters. As it is apparent from Fig. 4(c), the quantitative agreement between calculations and experimental data is remarkably good.

This result has several important implications. First, the comparison shown in Fig. 4(c) relies on parameters extracted from completely different experiments, such as measurements of contact resistance and infrared spectroscopy. Therefore, the agreement found in our analysis of $\delta V_{\mathrm{Th}}(L)$ indicates that our description of the electronic properties of rubrene is internally consistent at a quantitative level. Second, our result indicates that describing the low-energy density of states in the valence band of rubrene in terms of the ''textbook'' expression for conventional inorganic semiconductors is a good approximation. Third, and more in general, this work shows how ''simple'' measurements of FET electrical characteristics can be used to extract microscopic parameters—e.g., the carrier effective mass—that are not otherwise easily accessible experimentally.

The analysis of the threshold voltage behavior as a function of source-drain bias confirms that the shift in V_T is due to space charge injected from the contact into the semiconductor. In this case, we estimate the amount of charge injected into the semiconductor as $C_C V_{DS}$, where C_C is the capacitance between the injecting electrode and the rubrene crystal (this concept is identical to that used in the description of space-charge limited current $I - V$ curves [16]). By reasoning analogously to the case of the L dependence, we then obtain

$$\delta V_T(V_{DS}) = \frac{C_C}{C_G} V_{DS} = \frac{\epsilon_C}{\epsilon_D} \frac{t_C t_D}{L^2} V_{DS}, \qquad (5)$$

where, for the capacitance between contact and crystal, we have taken as a very simple approximation the expression of a parallel plate capacitance.

Equation (5) predicts that the shift of threshold voltage is linear in source-drain voltage, which is the case for $V_{DS} > kT/q$ (see Fig. 3), and that the slope of this linear relation should scale with the separation between source and drain as L^{-2}, as found experimentally [see the inset in Fig. 4(c)]. From the linear relation between $d[\delta V_T(V_{DS})]/dV_{DS}$ and L^{-2}, we extract the value of $\epsilon_C t_C t_D/\epsilon_D$, which is comparable to that obtained by directly measuring the crystal thickness (deviations of a factor of 2–3 are found in different samples, as can be expected given the crude estimates of the capacitances).

Note that all of the effects that we have investigated here scale inversely to the gate capacitance C_G [see Eq. (4) and (5)]. This is a typical signature of the so-called short-channel effects, which are well-known in silicon devices [21]. What is remarkable in our organic transistors is that, owing to the low doping concentration, these effects dominate already at a fairly large channel length ($L \simeq 1$–$2\ \mu$m), i.e., length scales which are typical of devices used in practical applications [22].

In summary, rubrene single-crystal FETs are sufficiently stable and reproducible to perform systematic investigations of threshold voltage shift. From the length dependence of this shift, we have extracted information about the microscopic properties of rubrene, such as density of states and a quantitative estimate for the effective mass in the valence band. In conjunction with a variety of earlier experiments—infrared spectroscopy and quantitative studies of bias and temperature-dependent contact resistance—our results show that our current picture for the understanding of organic semiconductors does account for many experimental observations in a way that is internally consistent at a quantitative level.

We gratefully acknowledge A. S. Molinari for help with the experiments. A. F. M. also gratefully acknowledges financial support from the Dutch NWO-VICI program, from the Swiss NCCR MaNEP, and from NEDO.

[1] R. W. I. de Boer *et al.*, Phys. Status Solidi A **201**, 1302 (2004).
[2] M. E. Gershenson *et al.*, Rev. Mod. Phys. **78**, 973 (2006).
[3] V. C. Sundar *et al.*, Science **303**, 1644 (2004).
[4] V. Podzorov *et al.*, Phys. Rev. Lett. **93**, 086602 (2004).
[5] A. F. Stassen *et al.*, Appl. Phys. Lett. **85**, 3899 (2004).
[6] I. N. Hulea *et al.*, Nature Mater. **5**, 982 (2006).
[7] S. Fratini *et al.*, New J. Phys. **10**, 033031 (2008).
[8] V. Podzorov *et al.*, Phys. Rev. Lett. **95**, 226601 (2005).
[9] K. P. Pernstich *et al.*, Nature Mater. **7**, 321 (2008).
[10] A. S. Molinari *et al.*, Appl. Phys. Lett. **92**, 133303 (2008).
[11] Z. Q. Li *et al.*, Phys. Rev. Lett. **99**, 016403 (2007).
[12] M. Matters *et al.*, Synth. Met. **102**, 998 (1999); H. L. Gomes *et al.*, Appl. Phys. Lett. **84**, 3184 (2004); T. Richards and H. Sirringhaus, Appl. Phys. Lett. **92**, 023512 (2008).
[13] C. Reese and Z. Bao, Adv. Funct. Mater. **19**, 763 (2009).
[14] R. W. I. de Boer *et al.*, Appl. Phys. Lett. **83**, 4345 (2003).
[15] A. S. Molinari *et al.*, Appl. Phys. Lett. **90**, 212103 (2007).
[16] A. Lampert and P. Mark, *Current Injection in Solids* (Academic, New York, 1970).
[17] N. W. Ashcroft and N. D. Mermin, *Solid State Physics* (Sounders College, Philadelphia, 1976), Chap. 28.
[18] T. Kaji *et al.* Adv. Mater. (to be published).
[19] J. H. Worne *et al.*, Nano Res. **1**, 341 (2008).
[20] In Ref. [10], we demonstrate that the energy level alignment at a Cu/CuO$_x$/rubrene interface essentially follows the Schottky-Mott limit. This is due to the presence of the CuO$_x$ tunnel barrier, which causes a weak coupling between the metal and molecules, resulting in a small density of interfacial states (5×10^{11}–1×10^{12} eV^{-1} cm^{-2}).
[21] N. Arora, *MOSFET Models for VLSI Circuit Simulation, Theory and Practice* (Springer-Verlag, Berlin, 1993), Chap. 5.
[22] G. H. Gelinck *et al.*, Nature Mater. **3**, 106 (2004).